PERGAMON

International Journal of Solids and Structures 39 (2002) 547–557

INTERNATIONAL JOURNAL OF SOLIDS and STRUCTURES

www.elsevier.com/locate/ijsolstr

Three-dimensional effects near the interface in a functionally graded Ni–Al_2O_3 plate specimen ☆

Hugh A. Bruck [a,*], Alan L. Gershon [b]

[a] *Department of Mechanical Engineering, University of Maryland, College Park, MD 20742, USA*
[b] *Department of Mechanical Engineering, Columbia University, 200 W. 109th Street, New York, NY 10025, USA*

Received 27 October 1998

Abstract

Functionally graded materials composed of nickel–Al_2O_3 composites with a variety of compositions and microstructures have been fabricated at the Idaho National Engineering and Environmental Laboratories. Finite element analysis has been utilized to numerically model the residual stress distribution in a graded nickel–Al_2O_3 joint, primarily for the purpose of optimizing the architecture of the interface to resist failure. In this paper, the applicability of using computationally efficient two-dimensional (2-D) analyses for modeling complicated three-dimensional (3-D) plate geometries are quantified for a specimen consisting of nickel and alumina plates joined by a 60 vol% Ni particulate reinforced composite interlayer to form a functionally graded joint. A 2-D generalized plane strain model is also introduced for comparison. Overall, the results indicate that the generalized plane strain model with or without rotation of the rigid bounding planes provides the most accurate description of the 3-D stress state, especially at the corner interface within the elastic region. However, the plane stress model predictions are slightly better in the ductile regions while the plane strain model predictions are better along the edge of the interface in the elastic region. Furthermore, 3-D effects are prevalent at distances within approximately 1/2 of the specimen thickness from the edge singularity in the elastic region of the specimen on the free surface and within 1/8 of the specimen thickness below the free surface. In addition, the intensity of the stresses near the corner of the 3-D model appears to increase as the specimen thickness increases, and is greater than the intensity of the stresses predicted at corresponding locations in the 2-D models. © 2001 Published by Elsevier Science Ltd.

Keywords: Functionally graded materials; Metal-ceramic composites; Thermal residual stresses; Elastoplastic finite element analysis; Generalized plane strain; Plane stress

1. Introduction

The thermomechanical behavior of a joint has a significant effect on its structural integrity. In particular, the effects of thermal stresses (induced, for example, during operation or manufacturing) on the fracture

☆ Research supported by the US Department of Energy, Office of Basic Energy Sciences, under DOE Idaho Operations Office contract DE-AC07-94ID13223.

* Corresponding author. Fax: +1-301-314-9477.
E-mail address: bruck@eng.umd.edu (H.A. Bruck).

0020-7683/01/$ - see front matter © 2001 Published by Elsevier Science Ltd.
PII: S0020-7683(01)00220-7

behavior of the joint are of interest. These effects are most pronounced when investigating joints composed of materials with vastly dissimilar material properties, such as metal/ceramic, metal/epoxy, and carbon fiber/epoxy. The effects of residual stresses on crack growth behavior have been previously studied in brazed (He and Evans, 1991; Bartlett et al., 1991; Kweon and Choi, 1995), coated (Drory et al., 1988; Charalambides and Evans, 1989; Howard et al., 1994), and adhesive joints (Fleck et al., 1991; Akisanya and Fleck, 1992; Daghhiyani et al., 1996). These studies have concluded that the residual stresses have a significant effect on the crack growth behavior, usually reducing the fracture toughness of the joint.

Recently, research has focused on optimizing joint strength by grading the material properties within the joint region to form a functionally graded joint. Analytical and numerical attempts to characterize the stress distributions and crack growth behavior within the joints have primarily centered around one- and two-dimensional (2-D) models (Lee and Erdogan, 1995; Giannakopoulos et al., 1995; Watanabe et al., 1991; Williamson et al., 1993; Rabin et al., 1998). For cylindrical joints, axisymmetric 2-D analyses can provide reasonably accurate predictions of residual stress distributions (Giannakopoulos et al., 1995; Williamson et al., 1993; Rabin et al., 1998). However, for joints with plate geometries, three-dimensional (3-D) models may be necessary for accurate predictions. Numerical attempts to predict residual stress distributions in graded plate joints have typically used approximate 2-D models (Lee and Erdogan, 1995; Giannakopoulos et al., 1995). However, the accuracy of these models has not been verified either numerically or experimentally. Proper modeling of the residual stresses is critical to understanding the fracture behavior of graded joints, especially when the effects of out-of-plane bending deformations induced by the thermal expansion mismatch are considered.

In this paper, a 3-D model is utilized to predict the residual stress distribution in a joint composed of a nickel and alumina plate joined by a 60 vol% Ni particulate reinforced composite interlayer. The results from this model are then compared with results from three different 2-D approximations: plane stress, plane strain, and generalized plane strain. To determine which approximation is most appropriate, often referred to as 3-D effects, stresses that have the most influence on interfacial failure will be analyzed in the joint. For example, in the alumina portion of the joint, the σ_{22} singularity initiates debonding, while the Mises stress distribution indicates the level of constraint imposed on cracks growing transversely to the interface in the nickel and composite regions.

2. Model description

2.1. Approach

The numerical model used in this work consists of a thermomechanical, elastoplastic finite element methodology that was previously developed and experimentally validated at the Idaho National Engineering and Environmental Laboratories for optimizing thermal residual stress distributions in functionally graded Ni–Al_2O_3 joints (Williamson et al., 1993; Rabin et al., 1998). Continuum models were used to compute the strains and stresses that develop in Ni–Al_2O_3 specimens as they are cooled to room temperature from an assumed fabrication temperature of 1100 K. Uniform cooling (i.e., no thermal gradients) was assumed and time-dependent material properties (i.e., creep phenomena) were not considered. These assumptions would reasonably correspond to the situation expected, for example, with relatively fast cooling in a furnace after high-temperature diffusion bonding.

Numerical solutions were obtained with the ABAQUS computer program (ABAQUS, 1996). ABAQUS uses a finite element numerical approach to obtain solutions to the partial differential equations of equilibrium in Lagrangian form. Since the material response involves nonlinear plastic behavior, solutions were obtained as a series of cooling increments, allowing iterations within each increment to obtain equilibrium.

Approximately 15 increments were required for a typical calculation. All simulations utilized second order (quadratic) reduced integration elements.

For the 2-D analyses, three different geometric approximations were investigated. These are (a) plane stress, (b) plane strain, and (c) generalized plane strain. While either plane stress or plane strain are typically used for 2-D modeling, the generalized plane strain may be more suitable for thermomechanical problems where thermal expansion mismatch exists. The reason for this stems from the model's ability to relieve some of the out-of-plane constraint imposed by the plane strain model while accommodating the level of constraint expected from the thermal expansion mismatch. The generalized plane strain model will be discussed in more detail in Section 2.3.

2.2. Specimen geometry and numerical formulation

The specimen geometry chosen for this model was a flat plate 25×25 mm^2 with a variable thickness (Fig. 1). The material comprising the model consisted of equal size Ni and Al_2O_3 sections joined by a 4 mm wide section of 60%Ni–40%Al_2O_3 particulate reinforced composite. Mechanical properties for each material were measured and are shown in Table 1 (Bruck and Rabin, 1999). The geometry and materials used in this model are the same as will be used in the manufacture of functionally graded Ni–Al_2O_3 compact tension specimens for fracture testing.

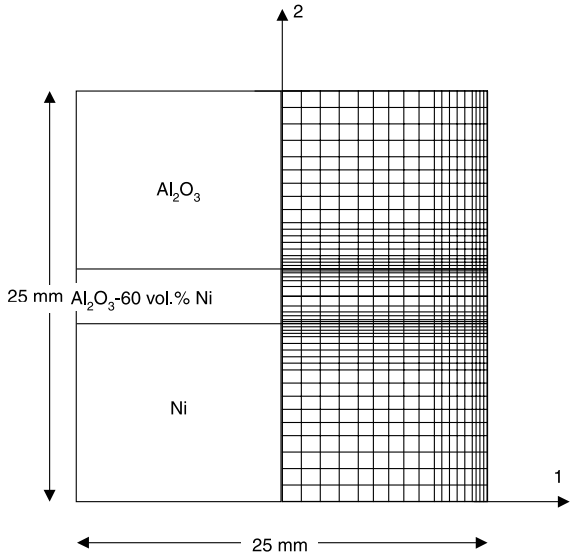

Fig. 1. FGM specimen configuration and meshing used for 2-D FEM.

Table 1
Material properties used in FEM simulations

Material	300 K				900 K			
	E (GPa)	v	σ_y (MPa)	$\sigma_{2\%}$ (MPa)	E (GPa)	v	σ_y (MPa)	$\sigma_{2\%}$ (MPa)
Ni	208	0.31	18	75	166	0.31	15.3	94.8
Composite	219	0.29	80	192	171	0.29	56	63.8
Al_2O_3	380	0.25	N/a	N/a	380	0.25	N/a	N/a

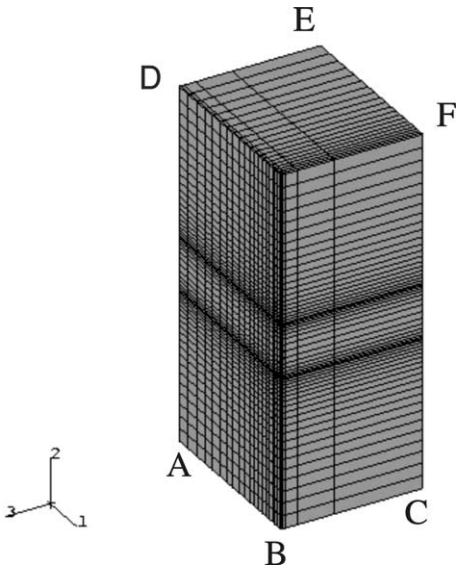

Fig. 2. Meshing used for 3-D FEM.

The use of a single composite material for the interlayer in the numerical model and fracture tests is motivated by the need to establish a tractable methodology that accounts for the effects of thermal residual stresses on the fracture behavior of functionally graded materials (FGMs). By minimizing the number of interfaces and materials that comprise the FGM, it is easier to distinguish errors that may be made in developing the methodology. This approach was used in previous efforts to validate modeling of thermal residual stress fields in FGMs (Rabin et al., 1998).

The mesh used for all 2-D analyses is shown in Fig. 1. The left boundary of the mesh corresponds to an axis of symmetry and therefore was fixed in the horizontal direction. All other boundaries were free, thus bending was permitted during cooling. The rectangular mesh for the graded specimen consisted of 21 rows of elements in the Ni and Al_2O_3 sections, 14 rows in the interlayer, and 20 columns of elements through the half-width of the specimen. The mesh was refined near the graded interfaces and the free surface of the specimen since the largest stress and strain gradients occur in these regions.

For the 3-D finite element analyses, the 2-D mesh was extruded into five layers spanning from the free surface of the specimen to the plane of symmetry (Fig. 2). The two free surfaces of the specimen are defined by the set of points ABD and BCF, while the two symmetric surfaces are defined by the set of points ADE and CEF. As in the 2-D case, the layers were refined near the free surface of the specimen where the largest stress and strain gradients were expected. Since 3-D effects on 2-D stress states may vary with specimen thickness, specimens with thicknesses of 3 and 20 mm were analyzed in this investigation.

2.3. Generalized plane strain

In the generalized plane strain approximation, it is assumed that the model lies between two bounding planes that may move as rigid bodies with respect to each other. This boundary condition is instituted in the standard 2-D model by the addition of two nodes (ABAQUS, 1996). The first node has a single degree of freedom that represents the relative out-of-plane displacement of the bounding planes. The second node has two degrees of freedom that permit out-of-plane rotation of the bounding planes. Combined, these nodes

provide a degree of freedom for out-of-plane strain that can vary only with in-plane position. The case where the bounding planes are required to remain stationary corresponds to plane strain.

The generalized plane strain model has many advantages over plane strain and plane stress. It permits a more accurate modeling of problems where specimen thickness is varying. Also, it allows for nonuniform thickness variations due to the loading condition. In the case of functionally graded joints, both conditions can apply.

While the generalized plane strain model permits out-of-plane strain, the final deformed configuration will only approximate the condition of equilibrium in the out-of-plane direction. Unless otherwise specified by the nodal boundary conditions, the deformed configuration for the rigid bounding planes will minimize out-of-plane loading. For the case of the functionally graded joint, the end result will be an induced out-of-plane bending moment due to differences in thermal contraction. For a very thick plate this condition will be appropriate. However, for a thin plate the bending moments will be minimized and this condition may not apply. Therefore, for this case it will be more appropriate to set the initial and final values of rotation for the bounding planes to zero so that they remain parallel during deformation. For the purpose of this investigation, both the generalized plane strain condition where the rotation of the bounding plane is constrained and the condition where it is unconstrained will be investigated.

3. Results and discussion

In order to determine 3-D effects on 2-D finite element models of functionally graded Ni–Al_2O_3 plate specimens for the purposes of optimizing the graded architecture to resist failure, it is necessary to identify those stresses which have the greatest influence on interfacial failure. In particular, there is a singularity in σ_{22} as the graded interface is approached that can precipitate interfacial debonding. Additionally, ductile base materials are often used in graded joints to arrest cracks growing transverse to the interface by dissipating energy through plastic work. This means that accurately modeling the level of constraint the interface imposes on the ductile regions of the joint, as indicated by the Mises stress distribution, will be important. Therefore, results for the σ_{22} singularity and Mises stress distribution become the focus for further analysis.

3.1. Singularity of σ_{22}

There is a singularity in the predicted stress state normal to the graded interface, σ_{22}, that is qualitatively similar for all three 2-D stress states. An example of the σ_{22} stress field can be seen in Fig. 3 for the plane

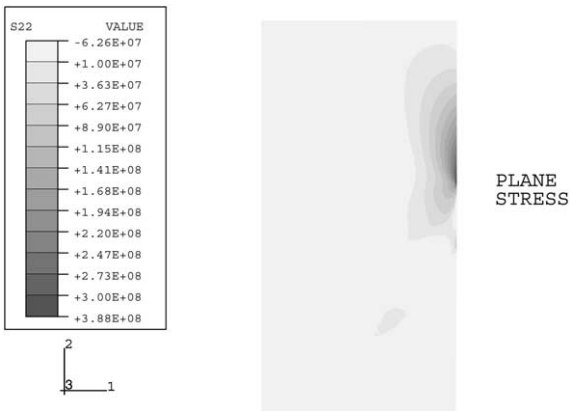

Fig. 3. The σ_{22} stress distribution for the plane stress case.

stress case. Previous numerical studies conducted on singularities have indicated that data obtained from within two elements of the singularity are erroneous (Whitcomb et al., 1982). Therefore, data from within these elements were excluded from the analysis.

The predictions for the σ_{22} stress field from the 3-D models are also qualitatively similar. An example of this stress field for the 3 mm thick specimen can be seen at the free and symmetric surfaces of in Fig. 4a and b respectively, while the symmetric side through the thickness direction is shown in Fig. 4c. Notice that a singularity exists along the entire interface at the free surface in the 3-D model, however it does not appear in the 2-D model. This singularity also appears to be most significant in the alumina at distances near the interface that are within 1/2 of the specimen's thickness. The pronounced presence of the singularity in the alumina is anticipated because of the alumina's higher strength and purely elastic behavior. The stress singularity is induced by differences in the thermal expansion normal to the direction of the singularity. Since out-of-plane deformation is only incorporated into the generalized plane strain model, only the in-plane component of deformation will contribute to the edge singularity in the plane stress and plane strain models. However, the singularities are identical for the two generalized plane strain cases, which would indicate that the singularity is insensitive to out-of-plane bending stresses near the interface.

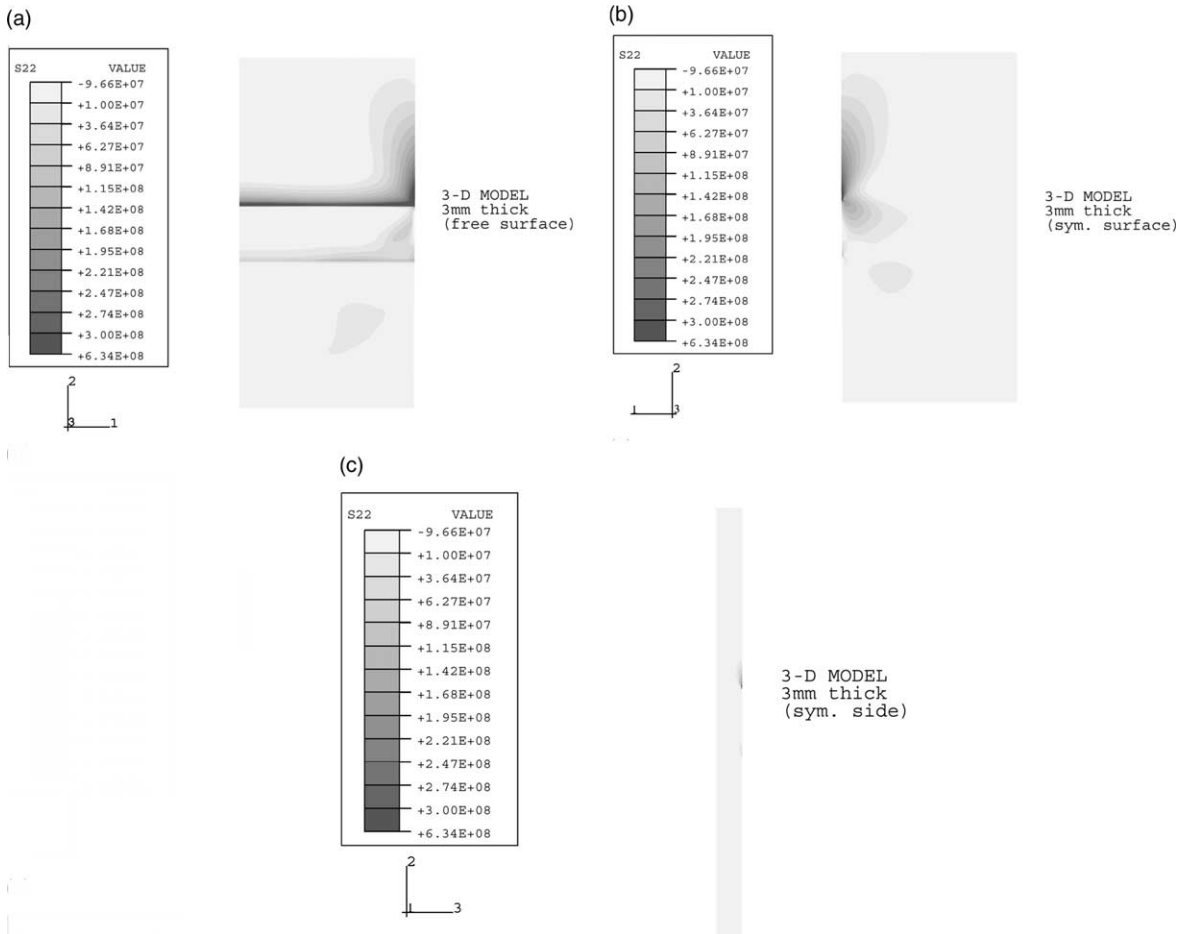

Fig. 4. The σ_{22} stress distribution for the (a) free, (b) symmetric surface, and (c) symmetric side of a 3 mm thick 3-D model.

It is important to note that the stress singularities along the interfaces for the 3-D models disappear quickly below the surface at a distance of approximately 1/8 of the specimen's thickness (see Fig. 4c). Thus, the 3-D effect along the interface seems to be restricted to the surface of the specimen and is not present on internal planes, such as the symmetric surface of the specimen (Fig. 4a and b). Since data from the two elements nearest the singularity were excluded and the 3-D models were only five elements thick, the convergence of the results had to be tested by increasing the mesh thickness to seven elements. The predicted stress distribution in the refined mesh did not change substantially from the coarse mesh results, thus it was determined that the coarse meshing was adequate for convergence. Previous numerical studies of singularities concluded that the major effect of mesh refinement was to reduce the size of the two elements nearest the singularity, thereby making it possible to acquire valid data closer to the singularity (Whitcomb et al., 1982).

The stress state at the free surface of all three 2-D models appears to correspond well to the singularity at the corner of the 3-D model. In order to obtain a more quantitative comparison of the predicted stress states for all of the models, a log–log plot of σ_{22} versus the radial distance normal to the interface, r, which has been normalized by half the specimen width, L, can be seen in Fig. 5a and b for the 3 mm thick and 20 mm thick specimens respectively. The motivation for this comparison comes from the asymptotic expression for the 2-D stress singularity at an interface between two purely elastic materials, as seen in Fig. 6 (Mizuno et al., 1988):

$$\sigma_{ij}(r,\theta) = \frac{K_L}{(r/L)^{\varpi}} f_{ij}(\theta) + \sigma_o f_{ijo}(\theta) \tag{1}$$

where K_L is the thermal stress intensity factor, ϖ is the stress singularity and so is a constant elastic stress term related to the thermal mismatch in the materials. While L is defined for the 2-D models, the choice for the 3-D models was not as apparent. It was decided that for the free edge singularities on the symmetric surfaces the width of the symmetric surface would be appropriate, while for the corner singularity the width of the wider surface intersecting the corner was used.

From these comparisons, it would appear that either case of the generalized plane strain model does the best job of predicting the corner singularity in the 3-D specimen. However, the stress singularity along the edge is also well predicted by the plane strain stress state. It is interesting to note that all of the singularities along the interface of the 3-D model correspond well to 2-D predictions if the appropriate width is used to

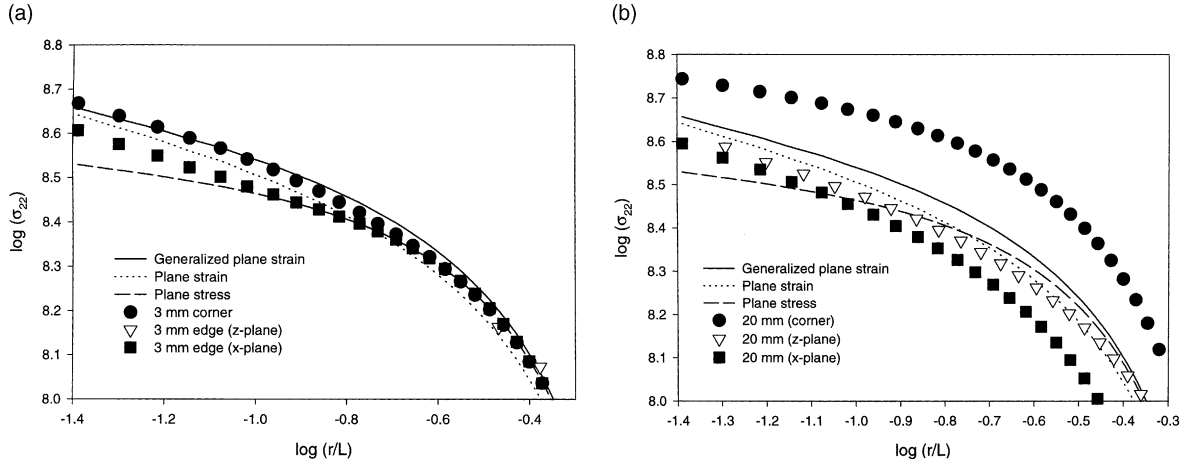

Fig. 5. The σ_{22} stress singularity for the (a) 3 mm thick and (b) 20 mm thick models compared with the 2-D models.

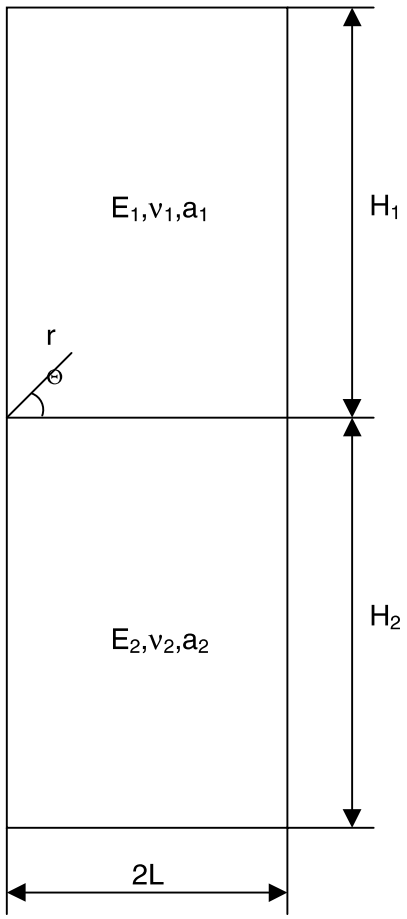

Fig. 6. Specimen configuration for the bimaterial problem.

normalize the radial distance, as in the asymptotic expression for the 2-D stress state near a purely elastic, bimaterial interface. Thus the 2-D models would appear to accurately predict the stress singularities in the 3-D models for internal planes normal to the interface.

Quantitatively, the intensity of the stresses at the corner of the 3-D models is equal to or greater than the intensity of the stresses at corresponding locations in the 2-D models. This result is consistent with Koguchi's results from 3-D boundary element simulations of bonded structures subjected to mechanical loading (Koguchi, 1997). Furthermore, the intensity of the corner stresses increases as the thickness increases.

3.2. Mises stress distribution

While the σ_{22} singularity appears to be appropriate for revealing 3-D effects in purely elastic materials like alumina, the Mises stress distribution is a more appropriate indication of 3-D effects in ductile portions of the specimen, such as the nickel and composite interlayer. The Mises stress distribution can be seen in Fig. 7a–d for the 2-D models. Results for the 3-D models were qualitatively similar between the 3 and 20 mm

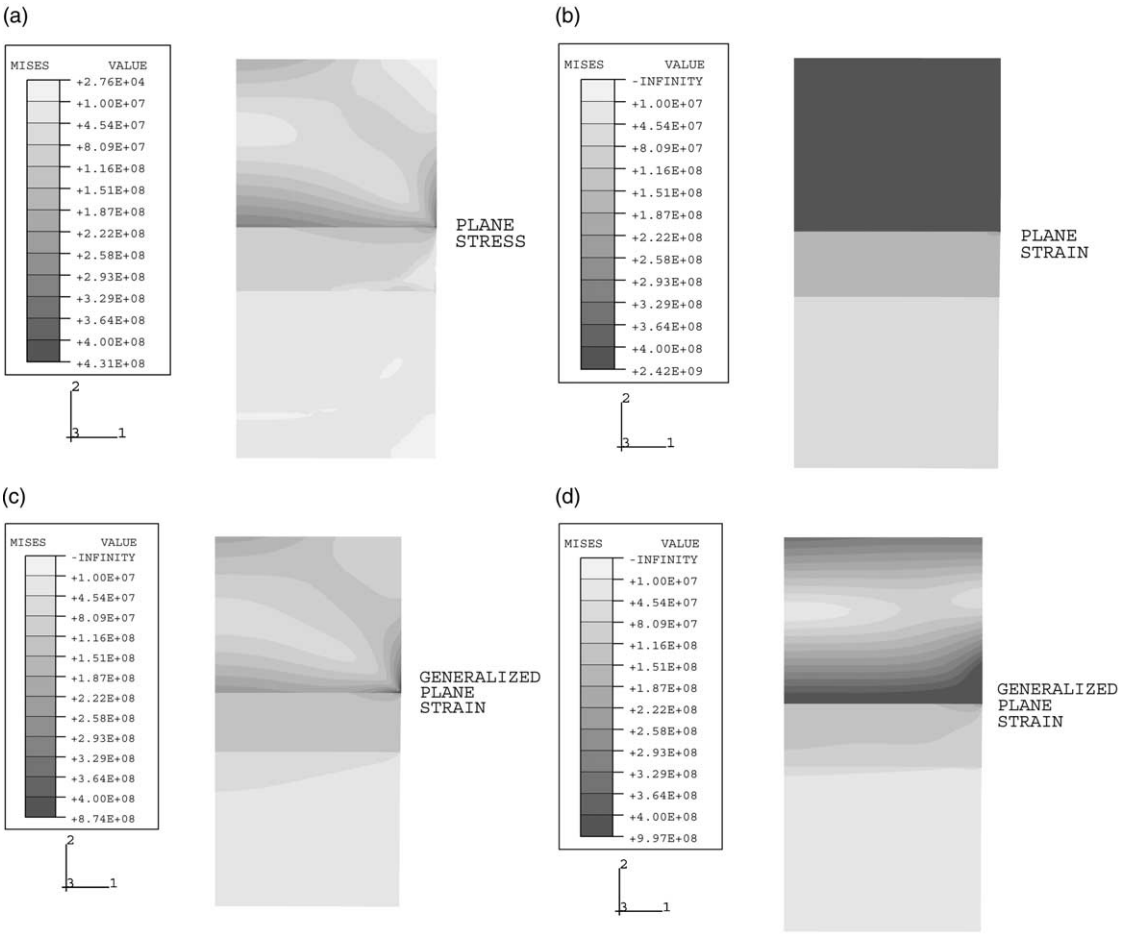

Fig. 7. The Mises stress distribution for the (a) plane stress, (b) plane strain, (c) generalized plane strain with parallel bounding planes, and (d) generalized plane strain with rotating bounding planes models.

thick specimens. Therefore, only the Mises stress distribution on the symmetric and free surfaces of the 20 mm thick specimens is shown in Fig. 8a and b for comparison with the 2-D models.

In Fig. 8, the Mises stress state does not change appreciably through the thickness of the 3-D model, even in the alumina portion of the model. The contributions of the σ_{22} stress singularity to the Mises stress on the free surface along the interface are evident in Fig. 8a. However, this singularity disappears on the symmetric surface (Fig. 4b), while the Mises stress still exhibits evidence of singularity contributions along the interface. These contributions come from the σ_{11} and σ_{33} bending stresses, which disappear on the free side and free surface respectively.

While the stress singularity in the alumina portion of the model is very apparent, the ductile portions appear to be characterized by much weaker or totally absent singularities. The reason for this can be attributed to the constitutive behavior of the ductile materials. While elastic stresses reach levels of over 400 MPa in the alumina portion, the ductile materials are much softer with yield stresses of less than 100 MPa. Thus, the stress singularity that appears in the alumina can be substantially relieved by plastic deformation in the ductile portions of the model resulting in much lower Mises stresses.

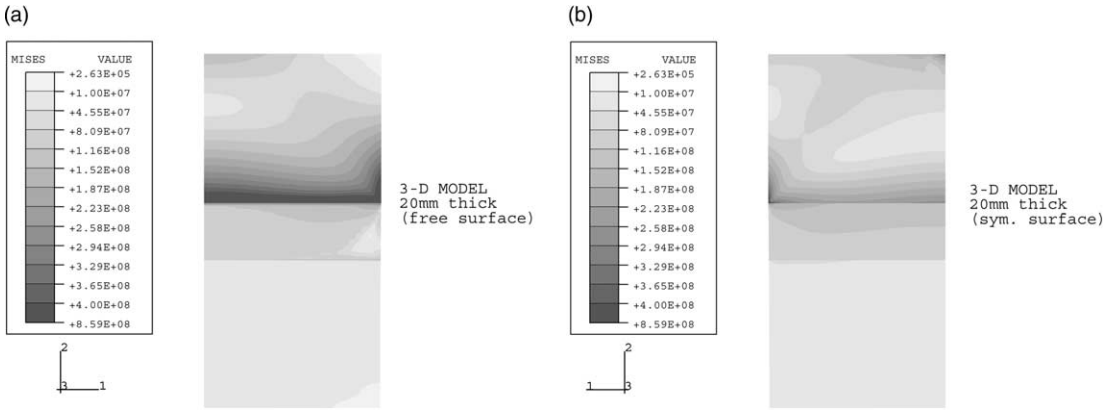

Fig. 8. The Mises stress distribution for the (a) free and (b) symmetric surfaces of the 20 mm thick 3-D model.

In the 2-D models, the significant out-of-plane stresses resulting from the plane strain approximation are apparent in the Mises stress (Fig. 7b). The constraint induced by the plane strain stress state generates plastic deformations which are much larger than those that appear in the 3-D case. In fact, this constraint is so great that the Mises stress becomes nearly constant within each component of the model. Comparison of the Mises stress distributions for the 3-D models and the plane stress and generalized plane strain models exhibit very good agreement. This is not unexpected since both the plane stress and generalized plane strain models are able to relieve the constraint imposed by the plane strain model, thereby reducing the level of plastic strain in the ductile portions of the specimens. However, the generalized plane strain case still imposes a slightly greater constraint on out-of-plane specimen deformations than the plane stress case. This constraint seems to be greater in the ductile region of the specimen when the bounding planes are not allowed to rotate. Permitting bounding plane rotation imposes less constraint in the ductile region, while inducing more out-of-plane bending stress in the elastic region. This condition may be appropriate for thicker specimens, as indicated by the results on the free surface of the 20 mm thick model in Fig. 8a. However, in general, neither case of the generalized plane strain model appears to be as appropriate as the plane stress model for modeling the 3-D Mises stress state.

4. Conclusions

From the results of this numerical investigation, it would appear that 3-D effects in the alumina portion of functionally graded nickel–Al_2O_3 joints are restricted to distances within 1/2 of the specimen thickness of the interface on the free surface of the specimen and to within 1/8 of the specimen thickness below the free surface. The σ_{22} singularity at the corner of the elastic portion in the 3-D models appears to be best predicted by the generalized plane strain model with or without rotation of the rigid bounding planes, while the plane strain model does a slightly better job predicting the edge singularities. However, the intensity of the stresses at the corner of the 3-D model is greater than the intensity of the stresses at corresponding locations in the 2-D models, and increases with increasing specimen thickness. In the ductile regions of the model, the plane stress model does the best job of predicting the 3-D Mises stress state, with the generalized plane strain model also providing adequate predictions. Overall, the generalized plane strain model is the most appropriate 2-D model for predicting the thermal residual stress distribution in a functionally graded Ni–Al_2O_3 plate specimen.

References

ABAQUS, 1996. Computer code ABAQUS, Hibbit, Karlsson, and Sorensen, Inc., Providence, RI, 1996.

Akisanya, A.R., Fleck, N.A., 1992. Analysis of a wavy crack in sandwich specimens. International Journal of Fracture 55, 29–45.

Bartlett, A., Evans, A.G., Ruhle, M., 1991. Residual stress cracking of metal/ceramic bonds. Acta Metallurgica et Materialia 39, 1579–1585.

Bruck, H.A., Rabin, B.H., 1999. Evaluating microstructural and damage effects in rule-of-mixtures predictions of the mechanical properties of Ni–Al_2O_3 composites for use in modeling functionally graded materials. Journal of Materials Science 34, 2241–2251.

Charalambides, P.G., Evans, A.G., 1989. Debonding properties of residually stressed brittle-matrix composites. Journal of the American Ceramic Society 72, 746–753.

Daghhiyani, H.R., Ye, L., Mai, Y.-W., 1996. Effect of thermal residual stress on the crack path in adhesively bonded joints. Journal of Materials Science 31, 2523–2529.

Drory, M.D., Thouless, M.D., Evans, A.G., 1988. On the decohesion of residually stressed thin films. Acta Metallurgica et Materialia 36, 2019–2028.

Fleck, N.A., Hutchinson, J.W., Suo, Z., 1991. Crack path selection in a brittle adhesive layer. International Journal of Solids and Structures 27, 1683–1703.

Giannakopoulos, A.E., Suresh, S., Finot, M., Olsson, M., 1995. Elastoplastic analysis of thermal cycling: layered materials with compositional gradients. Acta Metallurgica et Materialia 43, 1335–1354.

He, M.Y., Evans, A.G., 1991. Strength and fracture of metal/ceramic bonds. Acta Metallurgica et Materialia 39, 1587–1593.

Howard, S.J., Tsui, Y.C., Clyne, T.W., 1994. The effect of residual-stresses on the debonding of coatings. 1. A model for delamination at a bimaterial interface. Acta Metallurgica et Materialia 42, 2823–2836.

Koguchi, H., 1997. Stress singularity analysis in three-dimensional bonded structure. International Journal of Solids and Structures 34, 461–480.

Kweon, S.Y., Choi, S.K., 1995. Prediction of residual stress-induced cracking by finite element analysis. Scripta Metallurgica et Materialia 32, 359–364.

Lee, Y.D., Erdogan, F., 1995. Residual/thermal stresses in FGM and laminated thermal barrier coatings. International Journal of Fracture 69, 145–165.

Mizuno, K., Miyazawa, K., Suga, T., 1988. Characterization of thermal stresses in ceramic/metal joint. Journal of the Faculty in Engineering, Series B (University of Tokyo) 39, 401–412.

Rabin, B.H., Williamson, R.L., Bruck, H.A., Wang, X.-L., Watkins, T., Clarke, D.R., 1998. Residual strains in an Al_2O_3–Ni joint bonded with a composite interlayer: experimental measurements and FEM analysis. Journal of the American Ceramic Society 81, 1541–1549.

Watanabe, R., Kawasaki, A., Takahashi, Hd., 1991. Design, fabrication, and evaluation of functionally graded material for high temperature use. In: Baptiste, D. (Ed.), Mechanics and Mechanisms of Damage in Composites and Multi-materials. Mechanical Engineering Publications, London, pp. 285–299.

Whitcomb, J.D., Raju, I.S., Goree, J.G., 1982. Reliability of the finite element method for calculating free edge stresses in composite laminates. Computers and Structures 15, 23–37.

Williamson, R.L., Rabin, B.H., Drake, J.T., 1993. Finite element analysis of thermal residual stresses at graded ceramic-metal interfaces. Journal of Applied Physics 74 (2), 1310–1320.